Free vibration analysis of rectangular plates with variable thickness using a meshless method

(article starts on next page)

Free vibration analysis of rectangular plates with variable thickness using a meshless method

Reza Pilafkan [a] [iD],*, Peter D. Folkow [b]

[a] *Department of Mechanical Engineering, University of Mohaghegh Ardabili, Ardabil, Iran*
[b] *Department of Applied Mechanics, Chalmers University of Technology, Hörsalsvägen 7, SE-412 96 Göteborg , Sweden*

ARTICLE INFO

ABSTRACT

This paper presents a comprehensive study on the free vibration analysis of rectangular plates with variable thickness, utilizing three-dimensional elasticity theory and a meshless method. Traditional plate theories, such as classical and shear deformation theories, often fail to provide accurate results for thick plates or those with complex geometries. To overcome these limitations, the study adopts the three-dimensional elasticity approach, which considers the full material behavior and the entire plate structure. The meshless method, specifically the Radial Point Interpolation Method (RPIM) with multi-quadrics radial basis functions, is employed to solve the vibration problem. This method offers advantages over traditional finite element methods by using scattered nodes and higher-order shape functions, thus eliminating issues related to meshing and re-meshing. The plates' thickness is assumed to vary linearly and nonlinearly in one or both directions in the plate plane, and the study investigates the impact of different thickness ratios, aspect ratios, and boundary conditions on the natural frequencies of the plate. The results show that the meshless method provides a high degree of accuracy and fast convergence for both thin and thick plates with variable thickness, making it a reliable and efficient tool for free vibration analysis. This work thus contributes with valuable insights to the dynamic behavior of variable-thickness plates, with applications in many engineering fields where weight reduction and structural performance are critical. The work also provides eigenfrequency results on several plate structures with varying thickness, which may serve as a reference using 3D theory.

1. Introduction

Plates play a critical role as structural components in various engineering applications, making the study of their dynamic behavior essential for optimizing design. Most research on the free vibration of plates relies on simplified theories, such as classical plate theory [1–4], first-order shear deformation theory [5–9], and higher-order shear deformation theory [10–13], which include several assumptions regarding stress and displacement fields. However, to achieve more accurate results for thick plates, it is necessary to apply three-dimensional elasticity theory [14–17]. Analytical solutions become inadequate when dealing with complex geometries and boundary conditions, prompting the widespread use of numerical methods like the finite element method (FEM) and meshless methods (MM) in many practical scenarios [18–21]. In FEM, elements are connected via predefined nodes, while MM use scattered nodes that do not form a mesh. Moreover, MM employ higher-order shape functions that can vary with each point of interest, in contrast to the low-order predefined shape functions in FEM. As a result, MM address issues related to meshing and re-meshing

(adaptive analysis) more effectively than FEM, although MM generally incur higher computational costs and require careful selection of certain parameters.

Among the meshless methods, the Radial Point Interpolation Method (RPIM) stands out for its stability, even with arbitrary nodal distributions. RPIM's shape functions possess Kronecker delta behavior, facilitating the straightforward application of boundary conditions through an elimination approach. Previous studies, such as the static and free vibration analysis of moderately thick non-homogeneous plates using the meshless local radial point interpolation method [22], and free vibration analysis of laminated composite plates based on layer-wise theory [23], have demonstrated the versatility of meshless methods. Plates with variable thickness are particularly important in real-world engineering applications, where they enhance dynamic behavior and reduce structural weight. This is especially crucial in aerospace engineering, where reducing weight is essential due to high-speed operational demands. Although several studies have focused on variable-thickness plates [24–31], limited research has explored the
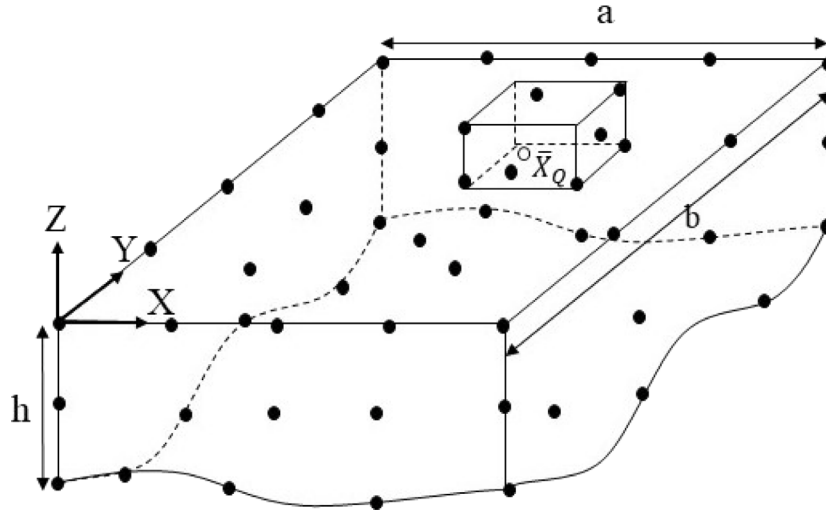

Fig. 1. Plate with variable thickness that is modeled using scattered nodes and the support domain.

free vibration analysis of rectangular plates based on three-dimensional theory [32].

In [5], the vibrations of rectangular Mindlin plates with linearly tapered thicknesses in one direction were analyzed using the spline strip method, which integrates exact solutions based on Mindlin plate theory. The two opposite edges, perpendicular to the direction of thickness variation, are simply supported, while the remaining two edges can have arbitrary boundary conditions. The transverse vibrations of rectangular plates with variable thicknesses have been explored with different boundary condition combinations at the four edges [1]. In [33], precise numerical calculations of the natural frequencies for elastic rectangular plates of variable thickness are presented, considering various boundary condition combinations and applying both first-order and higher-order theories. An efficient and accurate variational approach to study the vibration behavior of thin and thick plates with variable thickness, incorporating elastic restraints against both rotation and translation at the edges, is developed using the Ritz method in [3]. Linear and stepped thickness variations for plates are explored by utilizing the node-dependent kinematic approach of Carrera's unified formulation, alongside Lagrange expansion functions [34].

The work presented here aims to explore 3D solutions for free vibration behavior of rectangular plates with varying thickness, using RPIM with multi-quadrics radial basis functions. Here, the thickness of the plates is considered to vary linearly and nonlinearly in one or both directions in the plate plane. Eigenfrequency results are presented for both thin and thick plates, as well as the influence of different thickness ratios, aspect ratios, and boundary conditions. These results indicate that the proposed numerical method is both accurate and efficient and provide a reliable tool for the analysis of such structural problems.

2. RPIM

This section gives a brief description of the radial point interpolation method (RPIM). Consider a scalar field $\eta(\mathbf{x}, \mathbf{x}_Q)$ such as a displacement component. To interpolate a field function at a point $\mathbf{x}_Q = (x_Q, y_Q, z_Q)$ within a space V defined by an arbitrary distribution of N nodes, a support domain is considered. This domain, centered at $\mathbf{x}_Q$ can have any size and shape, as illustrated in Fig. 1, and contains a set of scattered nodes. In this approach, only the nodes located within the support domain are used to estimate the field function at the point $\mathbf{x}_Q$ while nodes outside the domain do not influence the interpolation at that point. RPIM employs radial and polynomial basis functions to perform the interpolation as described in [35]:

$$\eta(\mathbf{x}, \mathbf{x}_Q) = \sum_{i=1}^{n} R_i(\mathbf{x})a_i + \sum_{j=1}^{m} P_j(\mathbf{x})b_j = \mathbf{R}^T(\mathbf{x})\mathbf{a} + \mathbf{P}^T(\mathbf{x})\mathbf{b}. \tag{1}$$

In this context, n represents the number of radial basis functions and m the number of polynomial basis functions. $R_i(\mathbf{x})$ and $P_j(\mathbf{x})$ denote the radial and polynomial basis functions, respectively, while a_i and b_j are constants that need to be determined. The inclusion of polynomial functions $P_j(\mathbf{x})$ enhances both the accuracy and the stability of the interpolation.

The radial basis functions $R_i(\mathbf{x})$ depend on the distance r_i between $\mathbf{x}_Q$ and a node at $\mathbf{x}_i$

$$r_i = \sqrt{(x_Q - x_i)^2 + (y_Q - y_i)^2 + (z_Q - z_i)^2}. \tag{2}$$

A variety of radial basis functions are described in the literature, and the multiquadric (MQ) function used in this study takes the following form [35,36]:

$$R_i(\mathbf{x}) = (r_i^2 + (\alpha_c d_c))^{q_r}. \tag{3}$$

The parameters α_c and q_r are the shape parameters of the radial basis function, while d_c represents the average nodal spacing. The shape parameter q_r can be any real value, with $q_r = 0.98$ or 1.03 commonly yielding good results for solid and fluid mechanics, and α_c is typically a positive number less than 1.0 [35]. The average nodal spacing, d_c, is calculated as

$$d_c = \sqrt{d_{cx}^2 + d_{cy}^2 + d_{cz}^2}. \tag{4}$$

Here, d_{cx}, d_{cy} and d_{cz} represent the nodal spacings in the x, y and z directions, respectively. The polynomial basis functions for the 3D case are

$$\mathbf{P}^T(\mathbf{x}) = [1 \quad x \quad y \quad z \quad x^2 \quad xy \quad xz \quad ... \quad P_m(\mathbf{x})] \tag{5}$$

The vectors $\mathbf{a}$ and $\mathbf{b}$ associated with the point $\mathbf{x}_Q$ are determined by applying Eq. (1) at all n nodes within the support domain of $\mathbf{x}_Q$

$$\eta_k = \sum_{i=1}^{n} R_i(\mathbf{x_k})a_i + \sum_{j=1}^{m} P_j\mathbf{x_k}b_j \quad (k = 1, 2, \ldots, n). \tag{6}$$

Clearly η_k represents the value of the field function at the kth node. Eq. (6) can be rewritten in matrix form as

$$\hat{\boldsymbol{\eta}} = \hat{\mathbf{R}}\mathbf{a} + \hat{\mathbf{P}}\mathbf{b}, \tag{7}$$

where $\hat{\boldsymbol{\eta}}$ is a vector that encompasses field functions, such as the displacements, of all nodes within the support domain

$$\hat{\boldsymbol{\eta}} = [\eta_1, \eta_2, \ldots, \eta_n]^T. \tag{8}$$

Table 1
Eigenfrequencies for square homogeneous plates with CCCC boundary conditions.

N_z	N_x	N_y	h/b	Ref.	$\bar{\omega}_1$	$\bar{\omega}_2$	$\bar{\omega}_3$	$\bar{\omega}_4$	$\bar{\omega}_5$	$\bar{\omega}_6$	$\bar{\omega}_7$
5	36	36	0.1		3.328	6.359	6.359	8.922	10.522	10.622	12.536
	37	37			3.328	6.359	6.359	8.921	10.521	10.621	12.535
	38	38			3.328	6.358	6.358	8.921	10.520	10.620	12.535
6	36	36			3.328	6.358	6.358	8.919	10.517	10.618	12.535
	37	37			3.328	6.357	6.357	8.918	10.516	10.617	12.535
	38	38			3.327	6.357	6.357	8.917	10.515	10.616	12.535
				[37]	3.348	6.394	6.394	8.967	10.576	10.679	12.549
				[38]	3.326	6.356	6.356	8.919	10.519	10.619	12.536
				[39]	3.325	6.352	6.352	8.912	10.509	10.609	12.535
7	36	36	0.2		2.731	4.782	4.782	6.281	6.281	6.430	7.338
	37	37			2.731	4.781	4.781	6.281	6.281	6.430	7.337
	38	38			2.731	4.781	4.781	6.281	6.281	6.430	7.337
8	36	36			2.731	4.781	4.781	6.281	6.281	6.429	7.336
	37	37			2.731	4.780	4.780	6.280	6.280	6.429	7.336
	38	38			2.730	4.780	4.780	6.280	6.281	6.429	7.336
9	36	36			2.731	4.780	4.780	6.281	6.281	6.428	7.336
	37	37			2.730	4.780	4.780	6.281	6.281	6.428	7.335
	38	38			2.730	4.780	4.780	6.280	6.280	6.428	7.335
				[37]	2.745	4.802	4.802	6.288	6.288	6.454	7.364
				[38]	2.736	4.793	4.793	6.283	6.283	6.448	7.360
				[39]	2.729	4.777	4.777	6.280	6.280	6.425	7.332
7	36	36	0.5		1.554	2.447	2.447	2.518	2.518	2.979	3.203
	37	37			1.554	2.447	2.447	2.518	2.518	2.979	3.203
	38	38			1.554	2.447	2.447	2.518	2.518	2.979	3.203
8	36	36			1.553	2.445	2.445	2.518	2.518	2.979	3.201
	37	37			1.553	2.445	2.445	2.518	2.518	2.979	3.201
	38	38			1.553	2.445	2.445	2.518	2.518	2.979	3.201
9	36	36			1.553	2.444	2.444	2.518	2.518	2.979	3.199
	37	37			1.553	2.444	2.444	2.518	2.518	2.979	3.199
	38	38			1.553	2.444	2.444	2.518	2.518	2.979	3.199
				[37]	1.558	2.448	2.448	2.522	2.522	2.980	3.203
				[39]	1.551	2.442	2.442	2.518	2.518	2.980	3.165

Table 2
Eigenfrequencies for square homogeneous plates with SSSS boundary conditions.

N_z	N_x	N_y	h/b	Ref.	$\bar{\omega}_1$	$\bar{\omega}_2$	$\bar{\omega}_3$	$\bar{\omega}_4$	$\bar{\omega}_5$	$\bar{\omega}_6$	$\bar{\omega}_7$
7	36	36	0.1		1.936	4.626	4.626	6.526	6.527	7.108	8.668
	37	37			1.936	4.626	4.626	6.527	6.527	7.108	8.668
	38	38			1.935	4.626	4.626	6.526	6.526	7.108	8.668
8	36	36			1.935	4.625	4.625	6.525	6.525	7.105	8.664
	37	37			1.935	4.625	4.625	6.526	6.526	7.105	8.665
	38	38			1.935	4.625	4.625	6.526	6.526	7.106	8.665
9	36	36			1.935	4.625	4.625	6.526	6.526	7.106	8.665
	37	37			1.936	4.625	4.626	6.526	6.526	7.106	8.666
	38	38			1.935	4.625	4.625	6.526	6.527	7.106	8.666
				[37]	1.937	4.629	4.629	6.530	6.530	7.115	8.672
				[38]	1.936	4.627	4.627	6.530	6.530	7.111	8.672
				[39]	1.936	4.627	4.627	6.530	6.530	7.110	8.671
7	36	36	0.2		1.777	3.264	3.264	3.903	3.903	4.618	5.658
	37	37			1.777	3.264	3.264	3.903	3.903	4.617	5.658
	38	38			1.777	3.264	3.264	3.903	3.903	4.617	5.658
8	36	36			1.777	3.264	3.264	3.903	3.903	4.617	5.657
	37	37			1.777	3.264	3.264	3.903	3.903	4.617	5.657
	38	38			1.777	3.264	3.264	3.903	3.903	4.617	5.657
9	36	36			1.777	3.264	3.264	3.903	3.903	4.617	5.657
	37	37			1.777	3.264	3.264	3.903	3.903	4.618	5.657
	38	38			1.777	3.264	3.264	3.903	3.903	4.617	5.657
				[37]	1.778	3.265	3.265	3.904	3.904	4.617	5.660
				[38]	1.778	3.265	3.265	3.905	3.905	4.617	5.664
				[39]	1.778	3.265	3.265	3.903	3.903	4.617	5.658
7	36	36	0.5		1.261	1.305	1.305	1.847	2.335	2.335	2.609
	37	37			1.261	1.305	1.305	1.847	2.335	2.335	2.609
	38	38			1.261	1.305	1.305	1.847	2.335	2.335	2.610
8	36	36			1.260	1.305	1.305	1.847	2.334	2.334	2.610
	37	37			1.260	1.305	1.305	1.847	2.334	2.334	2.610
	38	38			1.260	1.305	1.305	1.847	2.334	2.334	2.610
9	36	36			1.260	1.305	1.305	1.847	2.334	2.334	2.610
	37	37			1.260	1.305	1.305	1.847	2.334	2.334	2.610
	38	38			1.260	1.305	1.305	1.847	2.334	2.334	2.610
				[37]	1.260	1.306	1.306	1.847	2.334	2.334	2.612
				[39]	1.260	1.306	1.306	1.847	2.333	2.333	2.612

Table 3
Convergence study of eigenfrequencies for square plates with linear thickness variation in the x direction $\alpha = 0.25$ for $h_0/b = 0.4$ and CCCC boundary conditions.

N_z	N_x	N_y	$\bar{\omega}_1$	$\bar{\omega}_2$	$\bar{\omega}_3$	$\bar{\omega}_4$	$\bar{\omega}_5$	$\bar{\omega}_6$	$\bar{\omega}_7$
9	31	31	1.758	2.859	2.860	3.716	4.224	4.285	4.958
	32	32	1.758	2.859	2.860	3.715	4.224	4.285	4.958
	33	33	1.758	2.859	2.861	3.716	4.224	4.285	4.958
	34	34	1.759	2.860	2.861	3.717	4.224	4.286	4.959
	35	35	1.756	2.856	2.859	3.716	4.222	4.283	4.955
10	31	31	1.758	2.858	2.860	3.717	4.223	4.285	4.957
	32	32	1.757	2.857	2.860	3.716	4.223	4.284	4.957
	33	33	1.757	2.857	2.860	3.716	4.222	4.284	4.956
	34	34	1.757	2.857	2.860	3.716	4.222	4.283	4.955
	35	35	1.757	2.857	2.859	3.716	4.222	4.283	4.955
11	31	31	1.757	2.858	2.860	3.716	4.222	4.284	4.956
	32	32	1.757	2.858	2.860	3.716	4.223	4.284	4.956
	33	33	1.756	2.856	2.859	3.716	4.222	4.283	4.955
	34	34	1.756	2.855	2.859	3.716	4.221	4.282	4.954
	35	35	1.756	2.854	2.858	3.716	4.220	4.281	4.952

The matrices $\widehat{\mathbf{R}}$ and $\widehat{\mathbf{P}}$ are defined as

$$\widehat{\mathbf{R}} = \begin{bmatrix} R_1(\mathbf{x_1}) & R_2(\mathbf{x_1}) & ... & R_n(\mathbf{x_1}) \\ R_1(\mathbf{x_2}) & R_2(\mathbf{x_2}) & ... & R_n(\mathbf{x_2}) \\ ... & ... & ... & ... \\ R_1(\mathbf{x_n}) & R_2(\mathbf{x_n}) & ... & R_n(\mathbf{x_n}) \end{bmatrix}, \tag{9}$$

$$\widehat{\mathbf{P}} = \begin{bmatrix} 1 & x_1 & y_1 & P_m(\mathbf{x_1}) \\ 1 & x_2 & y_2 & P_m(\mathbf{x_2}) \\ ... & ... & ... & ... \\ 1 & x_n & y_n & P_m(\mathbf{x_n}) \end{bmatrix}. \tag{10}$$

The system of equations in Eq. (6) consists of n equations and $n + m$ unknowns. Therefore, m additional equations are required, which can be provided by the following m constraint conditions to facilitate solving the system

$$\widehat{\mathbf{P}}^T \mathbf{a} = \mathbf{0}. \tag{11}$$

By combining Eqs. (7) and (11) gives a matrix form

$$\bar{\eta} = \begin{bmatrix} \widehat{\eta} \\ \mathbf{0} \end{bmatrix} = \begin{bmatrix} \widehat{\mathbf{R}} & \widehat{\mathbf{P}} \\ \widehat{\mathbf{P}}^T & \mathbf{0} \end{bmatrix} \begin{bmatrix} \mathbf{a} \\ \mathbf{b} \end{bmatrix} = \mathbf{G}\mathbf{a_0}, \tag{12}$$

where

$$\mathbf{a_0} = [a_1 \quad a_2 \quad ... \quad a_n \quad b_1 \quad b_2 \quad ... \quad b_n]^T. \tag{13}$$

Eq. (12) allows for the determination of $\mathbf{a_0}$

$$\mathbf{a_0} = \mathbf{G}^{-1}\bar{\eta}. \tag{14}$$

Since Eq. (1) can be expressed as

$$\eta = \mathbf{R}^T(\mathbf{x})\mathbf{a} + \mathbf{P}^T(\mathbf{x})\mathbf{b} = \left\{ \mathbf{R}^T(\mathbf{x}) \quad \mathbf{P}^T(\mathbf{x}) \right\} \mathbf{a_0}, \tag{15}$$

one obtains using Eq. (14)

$$\eta = \left\{ \mathbf{R}^T(\mathbf{x}) \quad \mathbf{P}^T(\mathbf{x}) \right\} \mathbf{G}^{-1}\bar{\eta} = \bar{\mathbf{\Psi}}^T(\mathbf{x})\bar{\eta}. \tag{16}$$

The RPIM shape functions are thus defined as

$$\begin{aligned} \mathbf{\Psi}^{\bar{T}}(\mathbf{x}) &= \left\{ \mathbf{R}^T(\mathbf{x}) \quad \mathbf{P}^T(\mathbf{x}) \right\} \mathbf{G}^{-1} \\ &= \begin{bmatrix} \phi_1(\mathbf{x}) & \phi_2(\mathbf{x}) & ...\phi_n(\mathbf{x}) & \phi_{n+1}(\mathbf{x}) & \phi_{n+2}(\mathbf{x}) & ...\phi_{n+m}(\mathbf{x}) \end{bmatrix}, \end{aligned} \tag{17}$$

where the shape function associated with the nodal displacement vector becomes

$$\mathbf{\Psi}^T(\mathbf{x}) = \begin{bmatrix} \phi_1(\mathbf{x}) & \phi_2(\mathbf{x}) & ...\phi_n(\mathbf{x}) \end{bmatrix}. \tag{18}$$

Eq. (16) can thus be expressed in an alternative form

$$\eta = \mathbf{\Psi}^T \widehat{\eta}, \tag{19}$$

and the spatial derivatives of η are given by

$$\eta_{,l} = \mathbf{\Psi}_{,l}^T \widehat{\eta}. \tag{20}$$

3. Governing equations

Consider a rectangular plate with non-uniform thickness, having length a and width b, as illustrated in Fig. 1. The plate's thickness is defined by the continuous function $h(x, y)$. A Cartesian coordinate system (x, y, z) is employed, where the associated displacement field is given by

$$\mathbf{u} = [u \quad v \quad w]^T. \tag{21}$$

Here, u, v and w represent the displacement components in the x, y and z directions, respectively. In accordance with 3D elasticity theory, the stress and strain components are expressed as

$$\boldsymbol{\sigma} = [\sigma_{xx} \quad \sigma_{yy} \quad \sigma_{zz} \quad \sigma_{yz} \quad \sigma_{xz} \quad \sigma_{xy} \quad]^T, \tag{22}$$

$$\boldsymbol{\varepsilon} = [\varepsilon_{xx} \quad \varepsilon_{yy} \quad \varepsilon_{zz} \quad \varepsilon_{yz} \quad \varepsilon_{xz} \quad \varepsilon_{xy} \quad]^T. \tag{23}$$

The relationship between stress and strain is

$$\boldsymbol{\sigma} = \mathbf{D}\boldsymbol{\varepsilon}, \tag{24}$$

where $\mathbf{D}$ represents the elastic material matrix

$$\mathbf{D} = \frac{E}{(1+\nu)(1-2\nu)} \begin{bmatrix} 1-\nu & \nu & \nu & 0 & 0 & 0 \\ \nu & 1-\nu & \nu & 0 & 0 & 0 \\ \nu & \nu & 1-\nu & 0 & 0 & 0 \\ 0 & 0 & 0 & 0.5-\nu & 0 & 0 \\ 0 & 0 & 0 & 0 & 0.5-\nu & 0 \\ 0 & 0 & 0 & 0 & 0 & 0.5-\nu \end{bmatrix}. \tag{25}$$

Here E denotes the elastic modulus, and ν represents Poisson's ratio. The relationship between strains and displacements is given by

$$\boldsymbol{\varepsilon} = \mathbf{L}\mathbf{u}, \tag{26}$$

where the operator matrix $\mathbf{L}$ is defined as

$$\mathbf{L}^T = \begin{bmatrix} \frac{\partial}{\partial x} & 0 & 0 \\ 0 & \frac{\partial}{\partial y} & 0 \\ 0 & 0 & \frac{\partial}{\partial z} \\ 0 & \frac{\partial}{\partial z} & \frac{\partial}{\partial y} \\ \frac{\partial}{\partial z} & 0 & \frac{\partial}{\partial x} \\ \frac{\partial}{\partial y} & \frac{\partial}{\partial x} & 0 \end{bmatrix}. \tag{27}$$

Adopting Hamilton's principle from variational calculus

$$\delta \int_{t_1}^{t_2} \bar{L} dt = 0. \tag{28}$$

Here the functional $\bar{L}$ is defined as

$$\bar{L} = \Pi + T - W \tag{29}$$

where Π and T represent the strain energy and kinetic energy, respectively

$$T = \int_V \rho \dot{\mathbf{u}}^T \dot{\mathbf{u}} dV, \tag{30}$$

$$\Pi = \int_V \boldsymbol{\varepsilon}^T \boldsymbol{\sigma} dV, \tag{31}$$

while the work done by external forces, including the potential body force $\mathbf{P}_b$ and surface force $\mathbf{P}_s$, is given by

$$W = \int_V \mathbf{u}^T \mathbf{P}_b dV + \int_S \mathbf{u}^T \mathbf{P}_s dS. \tag{32}$$

Table 4
Eigenfrequencies for square and rectangular plates with linear thickness variation in the x direction and SSSS boundary conditions.

| h_0/b	a/b	α	Ref.	$\bar{\omega}_1$	$\bar{\omega}_2$	$\bar{\omega}_3$	$\bar{\omega}_4$	$\bar{\omega}_5$	$\bar{\omega}_6$	$\bar{\omega}_7$
0.2	1	0.25		1.587	3.554	3.555	4.627	6.210	6.216	7.577
	2			1.022	1.584	2.449	3.247	3.645	4.275	5.875
0.4	1			1.306	2.581	2.586	3.543	4.089	4.097	4.813
	2			0.813	1.305	1.824	2.301	2.584	2.939	3.802
0.2	1	0.5		1.376	3.124	3.141	4.692	5.527	5.611	6.910
			[28] (FSDT)	1.374	3.110	3.128	4.661	5.488	5.566	6.844
0.4				1.177	2.399	2.400	3.249	3.676	3.845	4.610
			[28] (FSDT)	1.166	2.360	2.364	3.285	3.794	3.805	4.504
0.2	2			0.874	2.145	2.724	4.271	4.700	4.846	6.472
0.4				0.781	1.608	1.616	2.421	2.820	3.122	3.675

Table 5
Eigenfrequencies for square and rectangular plates with linear thickness variation in the x direction and CCCC boundary conditions.

| h_0/b	a/b	Ref.	$\bar{\omega}_1$	$\bar{\omega}_2$	$\bar{\omega}_3$	$\bar{\omega}_4$	$\bar{\omega}_5$	$\bar{\omega}_6$	$\bar{\omega}_7$
0.2	1		2.507	4.473	4.475	6.066	6.960	7.051	8.293
		[28] (FSDT)	2.476	4.405	4.405	5.965	6.877	6.880	8.139
		[28] (HSDT)	2.496	4.465	4.465	6.065	7.011	7.016	8.313
	1.5		1.959	2.863	4.105	4.225	4.808	5.908	6.719
	2		1.797	2.271	3.065	3.980	4.376	4.995	6.607
0.4	1		1.756	2.854	2.858	3.716	4.220	4.281	4.952
		[28] (FSDT)	1.718	2.784	2.786	3.657	4.128	4.129	4.811
		[28] (HSDT)	1.771	2.914	2.915	3.849	4.370	4.370	5.112
0.4	1.5		1.424	1.996	2.644	2.800	3.082	3.720	4.104
		[28] (FSDT)	1.394	1.952	2.732	2.577	3.004	3.627	3.982
		[28] (HSDT)	1.429	2.010	2.692	2.830	3.137	3.794	4.207
0.4	2		1.313	1.635	2.141	2.572	2.816	3.210	4.161
		[28] (FSDT)	1.285	1.601	2.094	2.505	2.751	3.128	3.930
		[28] (HSDT)	1.317	1.642	2.152	2.616	2.871	3.261	4.147

Table 6
Eigenfrequencies for square plates with linear thickness variation in both directions and CCCC boundary conditions.

h_0/b	α	β	Ref.	$\bar{\omega}_1$	$\bar{\omega}_2$	$\bar{\omega}_3$	$\bar{\omega}_4$	$\bar{\omega}_5$	$\bar{\omega}_6$	$\bar{\omega}_7$
0.1	0.25	0.25		2.608	5.082	5.097	7.269	8.604	8.682	10.538
			[28] (FSDT)	2.602	5.073	5.073	7.240	8.609	8.609	10.523
			[28] (HSDT)	2.605	5.083	5.083	7.261	8.636	8.636	10.564
0.2				2.280	4.136	4.154	5.675	6.250	6.254	7.828
			[28] (FSDT)	2.262	4.100	4.100	5.603	6.494	6.494	7.726
			[28] (HSDT)	2.275	4.142	4.142	5.676	6.592	6.592	7.857
0.4				1.670	2.756	2.765	3.712	4.103	4.166	4.829
			[28] (FSDT)	1.637	2.697	2.697	3.555	4.024	4.024	4.702
			[28] (HSDT)	1.677	2.799	2.799	3.711	4.219	4.219	4.949
0.1	0.25	0.5		2.221	4.340	4.389	6.320	7.377	7.519	9.229
			[28] (FSDT)	2.221	4.350	4.377	6.322	7.389	7.511	9.259
			[28] (HSDT)	2.222	4.355	4.383	6.333	7.402	7.527	9.284
0.2				1.999	3.691	3.718	5.146	5.930	6.006	7.177
			[28] (FSDT)	1.995	3.687	3.694	5.121	5.921	5.956	7.142
			[28] (HSDT)	2.003	3.712	3.721	5.170	5.980	6.021	7.232
0.4				1.544	2.595	2.612	3.462	3.910	3.967	4.613
			[28] (FSDT)	1.521	2.564	2.559	3.402	3.863	3.861	4.533
			[28] (HSDT)	1.548	2.637	2.634	3.523	4.009	4.011	4.726
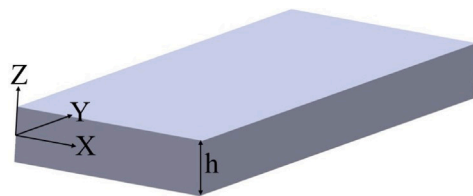
Fixed thickness
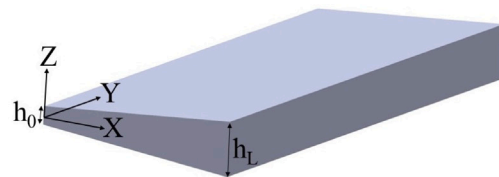
Linear variation thickness

Fig. 2. Homogeneous and linear variation of thickness plates.

Table 7

Eigenfrequencies for rectangular plates $a/b = 2$ with linear thickness variation in both directions and CCCC boundary conditions.

h_0/b	α	β	$\bar{\omega}_1$	$\bar{\omega}_2$	$\bar{\omega}_3$	$\bar{\omega}_4$	$\bar{\omega}_5$	$\bar{\omega}_6$	$\bar{\omega}_7$
0.1	0.25	0.25	1.808	4.450	4.492	6.878	8.286	8.394	9.876
0.2			1.624	3.680	3.786	4.940	6.191	6.199	7.570
0.4			1.238	2.035	2.102	3.341	3.573	3.581	4.152
0.1	0.25	0.5	1.534	3.811	3.828	5.959	6.963	7.219	8.733
0.2			1.415	3.286	3.356	4.408	5.578	5.579	6.839
0.4			1.132	2.470	2.560	2.935	3.930	3.934	4.597

Table 8

Eigenfrequencies for rectangular plates $a/b = 2$ and $h_0/b = 0.1$ with linear thickness variation in the x direction and CFFF boundary conditions.

Mode	[40] (Quasi 3D)	[40] (FEM 3D)	[28] (HSDT)	Present work
1	0.094	0.094	0.096	0.094
2	0.330	0.328	0.326	0.325
3	0.446	0.449	0.456	0.447
4	0.878	0.877	0.876	0.875

Table 9

Convergence study of eigenfrequencies for square plates with symmetric concave thickness variation $h_0/b = 0.4$, $\Delta = 1$ and CCCC boundary conditions.

N_z	N_x	N_y	$\bar{\omega}_1$	$\bar{\omega}_2$	$\bar{\omega}_3$	$\bar{\omega}_4$	$\bar{\omega}_5$	$\bar{\omega}_6$	$\bar{\omega}_7$
7	31	31	1.746	2.837	2.846	3.738	4.192	4.252	4.929
	32	32	1.745	2.833	2.846	3.738	4.189	4.250	4.928
	33	33	1.747	2.837	2.847	3.739	4.193	4.253	4.930
	34	34	1.747	2.837	2.847	3.739	4.193	4.254	4.931
	35	35	1.745	2.834	2.845	3.738	4.189	4.250	4.927
8	31	31	1.746	2.836	2.845	3.738	4.190	4.250	4.926
	32	32	1.745	2.834	2.844	3.737	4.187	4.248	4.924
	33	33	1.745	2.835	2.845	3.738	4.190	4.250	4.926
	34	34	1.746	2.836	2.845	3.737	4.190	4.250	4.926
	35	35	1.745	2.834	2.845	3.737	4.188	4.248	4.924
9	31	31	1.745	2.835	2.844	3.738	4.188	4.248	4.924
	32	32	1.744	2.833	2.843	3.737	4.186	4.246	4.921
	33	33	1.745	2.834	2.843	3.738	4.187	4.247	4.922
	34	34	1.745	2.834	2.843	3.738	4.188	4.248	4.923
	35	35	1.743	2.831	2.840	3.737	4.184	4.244	4.919

Assuming there are n nodes in the support domain of a specific point $\mathbf{x}_Q$ on the plate, the displacement field can be written in line with Eq. (19)

$$\mathbf{u} = [u \quad v \quad w]^T = \mathbf{N}\hat{\mathbf{u}}, \tag{33}$$

where $\mathbf{N}$ is the shape function matrix using Eq. (18)

$$\mathbf{N}^T = \begin{bmatrix} \phi_1 & 0 & 0 & \phi_2 & 0 & 0 & \dots & \phi_n & 0 & 0 \\ 0 & \phi_1 & 0 & 0 & \phi_2 & 0 & \dots & 0 & \phi_n & 0 \\ 0 & 0 & \phi_1 & 0 & 0 & \phi_2 & \dots & 0 & 0 & \phi_n \end{bmatrix}, \tag{34}$$

and $\hat{\mathbf{u}}$ represents the local displacement vector in accordance to Eq. (8)

$$\hat{\mathbf{u}} = \begin{bmatrix} u_1 & v_1 & w_1 & u_2 & v_2 & w_2 & \dots & u_n & v_n & w_n \end{bmatrix}^T. \tag{35}$$

By introducing the strain–displacement matrix operator $\mathbf{B} = \mathbf{LN}$, the strains and stresses can be expressed as

$$\varepsilon = \mathbf{B}\hat{\mathbf{u}}, \tag{36}$$

$$\sigma = \mathbf{DB}\hat{\mathbf{u}}. \tag{37}$$

Substituting this set of equations into the functional $\bar{L}$ Eq. (29) and adopting Hamilton's principle, the resulting system of equations becomes

$$\mathbf{M}\ddot{\mathbf{U}} + \mathbf{K}\mathbf{U} = \mathbf{F}. \tag{38}$$

Here, $\mathbf{U}$ and $\ddot{\mathbf{U}}$ represent the global displacement and acceleration vectors, respectively. The mass matrix, stiffness matrix, and force vector

are given by

$$\mathbf{M} = \int_V \rho \mathbf{N}^T \mathbf{N} dV, \tag{39}$$

$$\mathbf{K} = \int_V \mathbf{B}^T \mathbf{D} \mathbf{B} dV, \tag{40}$$

$$\mathbf{F} = \int_V \mathbf{N}^T \mathbf{P}_b dV - \int_S \mathbf{N}^T \mathbf{P}_s dS. \tag{41}$$

The equation to be solved for the free vibration analysis is

$$\mathbf{M}\ddot{\mathbf{U}} + \mathbf{K}\mathbf{U} = \mathbf{0}. \tag{42}$$

The solution is obtained using

$$\mathbf{U}(x, y, z, t) = \bar{\mathbf{U}}(x, y, z)e^{i\omega t}, \tag{43}$$

where ω represents the circular eigenfrequency of vibration. Substituting into Eq. (42), we obtain the standard eigenvalue equation

$$(\mathbf{K} - \omega^2 \mathbf{M})\bar{\mathbf{U}} = \mathbf{0}. \tag{44}$$

4. Results

In order to illustrate the RPIM applied to vibrational problems on plates with varying thickness, sets of 3D based eigenfrequencies for various boundary conditions are presented for different plate configurations. Comparisons are made with results presented in the literature, both based on simplified plate theories and 3D theory.

The plate is modeled by distributing N_x, N_y and N_z nodes in the x, y and z directions, respectively, so the total number of nodes on the boundary and inside the plate is $N = N_x * N_y * N_z$. Results are presented for homogeneous, linear, and nonlinear thickness variation plates where the length (x) and width (y) of the plate are denoted by a and b, respectively. The effects of different boundary conditions are considered, using clamped, simply supported, and free edges. These boundary conditions are defined as:

Clamped boundary conditions (C)

$$u(x, y, z, t) = v(x, y, z, t) = w(x, y, z, t) = 0, \quad \begin{cases} x = 0, a \\ y = 0, b \end{cases} \tag{45}$$

Simply supported boundary conditions (S)

$$\begin{aligned} v(x, y, z, t) = w(x, y, z, t) = 0, \quad & \sigma_{xx}(x, y, z, t) = 0, \quad & x = 0, a \\ u(x, y, z, t) = w(x, y, z, t) = 0, \quad & \sigma_{yy}(x, y, z, t) = 0, \quad & y = 0, b \end{aligned} \tag{46}$$

Free boundary conditions (F)

$$\begin{aligned} \sigma_{xx}(x, y, z, t) = \sigma_{xy}(x, y, z, t) = \sigma_{xz}(x, y, z, t) = 0, \quad & x = 0, a \\ \sigma_{yy}(x, y, z, t) = \sigma_{xy}(x, y, z, t) = \sigma_{yz}(x, y, z, t) = 0, \quad & y = 0, b \end{aligned} \tag{47}$$

4.1. Homogeneous and linear thickness variation

The geometry of both homogeneous and linearly varying thickness plates are illustrated in Fig. 2. In the latter case, linear variation may be in x and/or y directions where

$$h(x, y) = h_0(1 - \alpha\zeta)(1 - \beta\eta). \tag{48}$$

Here h_0 represents the thickness of the plate at $x = y = 0$ while $\zeta = x/a$ and $\eta = y/b$. Clearly $\alpha = \beta = 0$ corresponds to a homogeneous plate.

In order to illustrate the RPIM for a homogeneous plate, eigenfrequency results are presented for two different boundary conditions, CCCC and SSSS, for square plates with varying thickness-to-side ratios. Here a nondimensional natural frequency parameter $\bar{\omega} = (\omega b^2/\pi^2)\sqrt{\rho h/D}$ is introduced where ρ is the density and D is the plate flexural rigidity. These results are given in Table 1 and Table 2 for the first modes, illustrating convergence effects. The presented results are based on the fact that the number of nodes in the plane (N_x and N_y) affects the accuracy to a greater extent than the number of nodes in

Table 10

Eigenfrequencies for square plates with arched thickness variation and CCCC boundary conditions.

h_0/b	Δ	Ref.	$\bar{\omega}_1$	$\bar{\omega}_2$	$\bar{\omega}_3$	$\bar{\omega}_4$	$\bar{\omega}_5$	$\bar{\omega}_6$	$\bar{\omega}_7$
0.1	0.25		3.054	5.868	5.934	8.322	9.832	9.961	11.927
		[28] (FSDT)	3.042	5.837	5.899	8.271	9.793	9.872	11.857
		[28] (HSDT)	3.047	5.854	5.917	8.307	9.841	9.922	11.926
0.2			2.559	4.534	4.568	6.152	7.055	7.158	8.389
		[28] (FSDT)	2.534	4.478	4.510	6.068	6.982	7.016	8.259
		[28] (HSDT)	2.557	4.544	4.579	6.180	7.128	7.170	8.447
0.4			1.761	2.860	2.869	3.696	4.235	4.298	5.147
		[28] (FSDT)	1.732	2.795	2.807	3.679	4.152	4.161	4.837
		[28] (HSDT)	1.791	2.933	2.949	3.884	4.404	4.424	5.156
0.1	0.5		2.748	5.305	5.425	7.647	9.014	9.125	11.013
		[28] (FSDT)	2.742	5.291	5.406	7.622	8.986	9.077	10.976
		[28] (HSDT)	2.745	5.303	5.419	7.648	9.019	9.110	11.026
0.2			2.359	4.231	4.309	5.822	6.697	6.810	7.996
		[28] (FSDT)	2.343	4.195	4.270	5.766	6.641	6.712	7.903
		[28] (HSDT)	2.360	4.245	4.323	5.855	6.752	6.832	8.053
0.4			1.674	2.750	2.784	3.659	4.122	4.192	4.846
		[28] (FSDT)	1.655	2.704	2.736	3.588	4.055	4.081	4.742
		[28] (HSDT)	1.702	2.818	2.858	3.766	4.266	4.311	5.013

Table 11

Eigenfrequencies for square plates with concave thickness variation and CCCC boundary conditions.

h_0/b	Δ	Ref.	$\bar{\omega}_1$	$\bar{\omega}_2$	$\bar{\omega}_3$	$\bar{\omega}_4$	$\bar{\omega}_5$	$\bar{\omega}_6$	$\bar{\omega}_7$
0.1	0.25		2.843	5.453	5.528	7.796	9.166	9.310	11.249
		[28] (FSDT)	2.828	5.418	5.494	7.746	9.107	9.246	11.168
		[28] (HSDT)	2.832	5.430	5.508	7.773	9.141	9.284	11.221
0.2			2.445	4.355	4.389	5.945	6.815	6.908	8.146
		[28] (FSDT)	2.414	4.326	4.290	5.851	6.721	6.767	8.002
		[28] (HSDT)	2.431	4.380	4.341	5.941	6.837	6.893	8.159
0.4			1.745	2.835	2.844	3.738	4.188	4.248	4.924
		[28] (FSDT)	1.702	2.761	2.770	3.631	4.092	4.101	4.780
		[28] (HSDT)	1.750	2.877	2.893	3.810	4.311	4.332	5.060
0.1	0.5		2.292	4.348	4.540	6.437	7.324	7.731	9.402
		[28] (FSDT)	2.284	4.333	4.523	6.417	7.300	7.717	9.373
		[28] (HSDT)	2.285	4.338	4.529	6.429	7.312	7.736	9.397
0.2			2.070	3.728	3.831	5.238	5.955	6.125	7.290
		[28] (FSDT)	2.049	3.689	3.793	5.188	5.887	6.059	7.217
		[28] (HSDT)	2.057	3.713	3.823	5.239	5.942	6.136	7.316
0.4			1.592	2.633	2.656	3.504	3.937	3.989	4.654
		[28] (FSDT)	1.559	2.581	2.607	3.436	3.866	3.898	4.562
		[28] (HSDT)	1.587	2.652	2.691	3.563	4.005	4.064	4.768

Table 12

Eigenfrequencies for square plates with symmetric concave thickness variation and CCCC boundary conditions.

h_0/b	Δ	Ref.	$\bar{\omega}_1$	$\bar{\omega}_2$	$\bar{\omega}_3$	$\bar{\omega}_4$	$\bar{\omega}_5$	$\bar{\omega}_6$	$\bar{\omega}_7$
0.1	0.25		2.893	5.371	5.654	7.836	8.977	9.436	11.204
		[28] (FSDT)	2.883	5.341	5.613	7.782	8.920	9.364	11.127
		[28] (HSDT)	2.887	5.352	5.628	7.809	8.950	9.406	11.178
0.2			2.505	4.338	4.490	5.995	6.768	6.964	8.163
		[28] (FSDT)	2.465	4.270	4.406	5.889	6.659	6.824	8.010
		[28] (HSDT)	2.482	4.317	4.466	5.980	6.764	6.963	8.163
0.4			1.794	2.852	2.887	3.798	4.190	4.244	4.924
		[28] (FSDT)	1.741	2.776	2.815	3.657	4.089	4.125	4.795
		[28] (HSDT)	1.790	2.885	2.947	3.840	4.294	4.375	5.072
0.1	0.5		2.432	4.223	4.804	6.507	6.983	8.028	9.250
		[28] (FSDT)	2.437	4.218	4.791	6.492	6.969	7.997	9.233
		[28] (HSDT)	2.438	4.222	4.799	6.504	6.978	8.021	9.255
0.2			2.221	3.687	4.069	5.354	5.789	6.335	7.432
		[28] (FSDT)	2.185	3.644	3.987	5.269	5.727	6.214	7.313
		[28] (HSDT)	2.194	3.663	4.024	5.322	5.770	6.310	7.426
0.4			1.719	2.668	2.793	3.584	3.931	4.029	4.713
		[28] (FSDT)	1.660	2.605	2.714	3.498	3.843	3.959	4.596
		[28] (HSDT)	1.690	2.665	2.813	3.627	3.960	4.160	4.785

the thickness (N_z). It is clear that the results have stabilized for the number of nodes covered by the tables, and that an increased number of nodes N_z is justified for thicker plates.

The results have been compared with numerical solutions based on the Rayleigh–Ritz method for 3D theory [37–39]. The agreement is good with small deviations, especially for SSSS according to Table 2.

The more numerically challenging case CCCC (Table 1) gives larger deviations in the results (the mutual variation among [37–39] is also more prominent). The present results are in most cases lower than the ones based on Rayleigh–Ritz method, with the closest agreement with [39].

Table 13

Eigenfrequencies for square plates with arched thickness variation and SSSS boundary conditions.

h_0/b	Δ	$\bar{\omega}_1$	$\bar{\omega}_2$	$\bar{\omega}_3$	$\bar{\omega}_4$	$\bar{\omega}_5$	$\bar{\omega}_6$	$\bar{\omega}_7$
0.1	0.25	1.773	4.267	4.273	6.418	8.044	8.064	10.135
0.2		1.647	3.668	3.671	5.354	6.359	6.375	7.728
0.4		1.338	2.624	2.624	3.581	4.122	4.131	4.878
0.1	0.5	1.600	3.864	3.868	6.007	7.279	7.341	9.292
0.2		1.504	3.138	3.224	4.745	5.960	5.975	7.264
0.4		1.251	2.502	2.506	3.448	3.986	3.998	4.621

Table 14

Eigenfrequencies for square plates with concave thickness variation and SSSS boundary conditions.

h_0/b	Δ	$\bar{\omega}_1$	$\bar{\omega}_2$	$\bar{\omega}_3$	$\bar{\omega}_4$	$\bar{\omega}_5$	$\bar{\omega}_6$	$\bar{\omega}_7$
0.1	0.25	1.622	3.896	3.903	6.080	7.371	7.423	9.415
0.2		1.525	3.250	3.304	5.077	6.017	6.045	7.255
0.4		1.272	1.625	1.652	2.536	3.254	3.270	4.037
0.1	0.5	1.295	3.065	3.111	4.921	5.748	5.992	7.691
0.2		1.243	2.819	2.849	4.320	5.027	5.169	6.458
0.4		1.088	1.602	1.677	2.307	3.227	3.278	3.680

Table 15

Eigenfrequencies for square plates with symmetric concave thickness variation and SSSS boundary conditions.

h_0/b	Δ	$\bar{\omega}_1$	$\bar{\omega}_2$	$\bar{\omega}_3$	$\bar{\omega}_4$	$\bar{\omega}_5$	$\bar{\omega}_6$	$\bar{\omega}_7$
0.1	0.25	1.631	3.863	3.887	6.083	7.245	7.382	9.398
0.2		1.535	3.246	3.410	4.464	5.084	5.950	7.314
0.4		1.277	2.517	2.535	3.503	3.802	4.020	4.763
0.1	0.5	1.339	3.059	3.075	4.946	5.599	6.366	7.685
0.2		1.285	2.812	2.822	4.215	4.926	5.133	6.407
0.4		1.111	1.587	1.862	2.256	3.189	3.198	4.411

Next, consider linearly varying thickness plates. Here the nondimensional natural frequency parameter is defined as $\bar{\omega} = (\omega b^2/\pi^2)\sqrt{\rho h_0/D_0}$. Similarly to the homogeneous plate, the convergence effects are illustrated in Table 3 for square plates with linear thickness variation in the x direction and CCCC boundary conditions. As for the corresponding homogeneous case in Table 1, the results have essentially stabilized for the number of nodes covered by the tables. Here the number of nodes in the thickness direction N_z have been increased compared to Table 1, in order to better capture the effects from the varying thickness parameter.

Tables 4 and 5 show for one directional linear thickness variation how natural frequencies vary with respect to the thickness-to-side ratio for square and rectangular plates with SSSS and CCCC boundary condition, respectively. To validate the accuracy of the present work, the results are to be compared with those from the literature. Here there seem to be a lack of 3D results, so comparisons are made with two simplified theories [28]: the Mindlin's first-order shear deformation theory (FSDT), where transverse shear strains do not vary through the thickness, and the Reddy's higher-order shear deformation theory (HSDT), where transverse shear strain is estimated using second or higher-order terms in the thickness. As expected, results from HSDT are closer to the present 3D RPIM results when compared to FSDT. Moreover, discrepancies from 3D RPIM using simplified theories are more pronounced for higher modes and thicker plates.

More involved cases for plates with linear thickness variation in both x and y directions are illustrated in Tables 6 and 7. Here results assuming CCCC boundary conditions are presented for square and rectangular plates, respectively. The accuracies among the different theories in Table 6 are of the same order as in Table 5, with lower frequencies in Table 6 as expected (essentially thinner plates). Similar lower frequency results also occur for rectangular plates in Table 7 compared to Table 5. Such eigenfrequency investigations for plates

with thickness variation in two directions as in Table 7 do not appear to have been presented in the literature.

Yet another case is presented in Table 8 for a partially free plate. Here linear thickness variation in x direction is studied for CFFF boundary conditions for a rectangular plate. Comparisons are done with results studying this particular case through other methods, rendering similar results for each mode among the studied cases.

4.2. Non-linear thickness variation

Consider plates with nonlinear thickness variation. Here three distinct forms are to be investigated: concave, arched, and symmetric concave as illustrated in Fig. 3.

As noted, the thickness varies solely in the x-direction. The three forms are parametrically defined as

Arched form:

$$h(x, y) = h_0(1 - \Delta\zeta^2), \qquad \Delta = 1 - \frac{h_L}{h_0}. \tag{49}$$

Concave form:

$$h(x, y) = h_0(1 - 2\Delta\zeta + \Delta\zeta^2), \qquad \Delta = 1 - \frac{h_L}{h_0}. \tag{50}$$

Symmetric concave form:

$$h(x, y) = h_0(1 - 4\Delta\zeta + 4\Delta\zeta^2), \qquad \Delta = 1 - \frac{h_{0.5L}}{h_0}. \tag{51}$$

Here, h_L represents the thickness at $x = a$ and $h_{0.5L}$ denotes the thickness at the midpoint at $x = a/2$.

Table 9 illustrates the convergence effects for square plates with symmetric concave form in the x direction and CCCC boundary conditions. As for the corresponding homogeneous and linearly varying cases in Table 1 and Table 3 respectively, the results show a stabilizing behavior albeit slightly more fluctuating than in the simpler previous cases. Here the number of nodes in the thickness direction N_z was not increased further as in Table 3 due to numerical limitations.

Results for the three groups of nonlinear thickness forms are presented in Tables 10–12 for various thickness-to-side ratios and parameters Δ for square plates with CCCC boundary conditions. Due to lack of existing 3D results in the literature, comparisons are made with plates using FSDT and HSDT. Naturally, results from HSDT are generally closer to the present 3D RPIM results when compared to FSDT. The discrepancies from 3D RPIM using simplified theories are mostly more pronounced for higher frequencies.

Similarly, results for plates with SSSS boundary conditions are presented in Tables 13–15. Here, no comparisons seem to exist in the literature. As for the CCCC cases in Tables 10–12, lower frequencies occur for larger Δ as expected (essentially thinner plates). Naturally, the SSSS cases renders lower frequencies than the corresponding cases for CCCC due to different structural stiffening effects.

5. Conclusion

This paper studies eigenfrequency analysis of rectangular plates with variable thickness, using three-dimensional elasticity theory and the mesh-free method RPIM. This method offers advantages over traditional FEM by using scattered nodes and higher-order shape functions which eliminates problems related to meshing and re-meshing, and where the numerical procedure is effective rendering accurate solutions for low computational costs. As for the thickness variation of the plates, it is assumed to vary linearly and nonlinearly in the plane of the plate. The study investigates the vibrational effects from different thickness ratios, aspect ratios, and boundary conditions. The various eigenfrequencies are in several cases compared to results using other methods given in the literature. A few of these cited results are based on 3D solutions rendering similar frequencies as in this report. As for previously reported results using simplified plate theories, the present
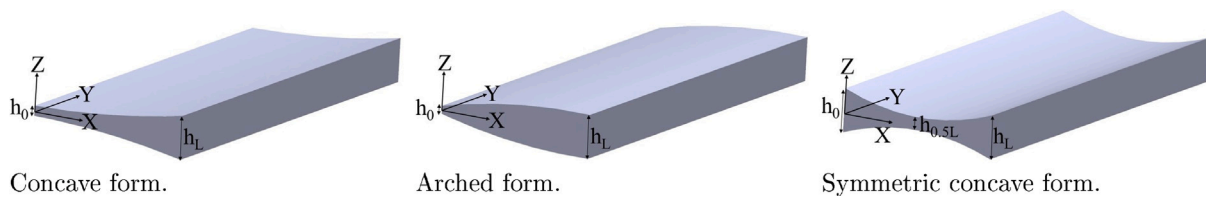
Fig. 3. Nonlinear variation of thickness plates.

eigenfrequencies differ for all modes. Consequently, the present results indicate that RPIM provides good accuracy and fast convergence for both thin and thick plates with variable thickness. The presented results may hereby serve as a reference for eigenfrequency studies of plate structures with varying thickness.

A possible continuation of the present work is to provide comprehensive sets of 3D benchmark solutions for various plate configurations (varying thickness ratio, aspect ratio, thickness function, boundary conditions). Moreover, vibrational studies related to plate shape optimization is a natural continuation of the methods used in this work. Since plates play a critical role as structural components in various engineering applications, accurate studies of vibrational modes are essential for design problems. Examples are in aerospace engineering where weight reduction and optimizing design using variable plate thickness may enhance structural dynamic behavior and reduce structural weight. Consequently, effective procedures calculating reliable results for eigenfrequencies and eigenmodes based on 3D theory may serve as a base for designing and evaluating advantageous thickness variation functions in plates.

CRediT authorship contribution statement

Reza Pilafkan: Writing – original draft, Supervision, Methodology, Formal analysis, Conceptualization. **Peter D. Folkow:** Writing – review & editing, Supervision, Conceptualization.

Declaration of competing interest

The authors declare that they have no known competing financial interests or personal relationships that could have appeared to influence the work reported in this paper.

Data availability

The data that has been used is confidential.

References

[1] B. Singh, Saxena V., Transverse vibration of rectangular plate with bi-directional thickness variation, J. Sound Vib. 198 (1) (1996) 51–65, http://dx.doi.org/10. 1006/jsvi.1996.0556.

[2] Y.X. Hao, Y.Y. Liu, W. Zhang, L.T. Liu, K.C. Sun, S.W. Yang, Natural vibration of cantilever porous twisted plate with variable thickness in different directions, Def. Technol. 27 (2023) 200–216, http://dx.doi.org/10.1016/j.dt.2022.12.004.

[3] S.A. Eftekhari, A.A. Jafari, Modified mixed Ritz-DQ formulation for free vibration of thick rectangular and skew plates with general boundary conditions, Appl. Math. Model. 37 (12–13) (2013) 7398–7426, http://dx.doi.org/10.1016/J.APM. 2013.02.040.

[4] V.N. Burlayenko, H. Altenbach, T. Sadowski, An evaluation of displacement-based finite element models used for free vibration analysis of homogeneous and composite plates, J. Sound Vib. 358 (2015) 152–175.

[5] Mizusawa T., Vibration of rectangular mindlin plates by the spline strip method, J. Sound Vib. 163 (2) (1993) 193–205, http://dx.doi.org/10.1006/JSVI.1993. 1160.

[6] T.T. Tran, Q.H. Pham, T. Nguyen-Thoi, Static and free vibration analyses of functionally graded porous variable-thickness plates using an edge-based smoothed finite element method, Def. Technol. 17 (3) (2021) 971–986, http: //dx.doi.org/10.1016/J.DT.2020.06.001.

[7] V. Kumar, S.J. Singh, V.H. Saran, S.P. Harsha, Vibration characteristics of porous FGM plate with variable thickness resting on pasternak's foundation, Eur. J. Mech. A Solids 85 (2021) 104124, http://dx.doi.org/10.1016/J.EUROMECHSOL. 2020.104124.

[8] V. Kumar, S.J. Singh, V.H. Saran, S.P. Harsha, Vibration analysis of the rectangular FG materials plate with variable thickness on Winkler-Pasternak-Kerr elastic foundation, Mater. Today: Proc. 62 (2022) 184–190, http://dx.doi.org/10. 1016/J.MATPR.2022.02.615.

[9] H.N. Jahromi, M.M. Aghdam, A. Fallah, Free vibration analysis of mindlin plates partially resting on pasternak foundation, Int. J. Mech. Sci. 75 (2013) 1–7, http://dx.doi.org/10.1016/J.IJMECSCI.2013.06.001.

[10] M. Marjanović, N. Kolarević, M. Nefovska-Danilović, M. Petronijević, Free vibration study of sandwich plates using a family of novel shear deformable dynamic stiffness elements: limitations and comparison with the finite element solutions, Thin-Walled Struct. 107 (2016) 678–694.

[11] Q. Guo, G. Shi, An accurate and efficient 4-noded quadrilateral plate element for free vibration analysis of laminated composite plates using a refined third-order shear deformation plate theory, Compos. Struct. 324 (2023) 117490, http://dx.doi.org/10.1016/J.COMPSTRUCT.2023.117490.

[12] M. Ji, J.J. Zhong, Y.C. Wu, Higher-order shear deformation theory for accurate prediction of vibration behavior of thick piezoelectric disks and design of efficient surface electrodes, Int. J. Solids Struct. 290 (2024) 112669, http://dx.doi.org/ 10.1016/J.IJSOLSTR.2024.112669.

[13] D. Singh, R. Kiran, R. Vaish, Vibration and buckling analysis of agglomerated CNT composite plates via isogeometric analysis using non-polynomial shear deformation theory, Eur. J. Mech. A Solids 98 (2023) 104892, http://dx.doi. org/10.1016/J.EUROMECHSOL.2022.104892.

[14] N. Ulbricht, A. Boldini, P. Zhang, M. Porfiri, Three-dimensional analytical solution of free vibrations of a simply supported composite plate in contact with a fluid, J. Sound Vib. 572 (2024) 118139, http://dx.doi.org/10.1016/J.JSV.2023. 118139.

[15] A. Rezaei Mojdehi, A. Darvizeh, A. Basti, H. Rajabi, Three dimensional static and dynamic analysis of thick functionally graded plates by the meshless local Petrov–Galerkin (MLPG) method, Eng. Anal. Bound. Elem. 35 (11) (2011) 1168–1180, http://dx.doi.org/10.1016/J.ENGANABOUND.2011.05.011.

[16] G. Jin, Z. Su, S. Shi, T. Ye, S. Gao, Three-dimensional exact solution for the free vibration of arbitrarily thick functionally graded rectangular plates with general boundary conditions, Compos. Struct. 108 (1) (2014) 565–577, http: //dx.doi.org/10.1016/J.COMPSTRUCT.2013.09.051.

[17] A. Alibeigloo, M. Alizadeh, Static and free vibration analyses of functionally graded sandwich plates using state space differential quadrature method, Eur. J. Mech. A Solids 54 (2015) 252–266, http://dx.doi.org/10.1016/J. EUROMECHSOL.2015.06.011.

[18] X.C. He, J.S. Yang, G.X. Mei, L.X. Peng, Bending and free vibration analyses of ribbed plates with a hole based on the FSDT meshless method, Eng. Struct. 272 (2022) 114914, http://dx.doi.org/10.1016/J.ENGSTRUCT.2022.114914.

[19] S. Hu, R. Zhong, Q. Wang, B. Qin, W. Shao, A strong-form Chebyshev-RPIM meshless solution for free vibration of conical shell panels with variable thickness and fiber curvature, Compos. Struct. 296 (2022) 115884, http://dx.doi.org/10. 1016/J.COMPSTRUCT.2022.115884.

[20] C. Martino, Maria Moruzzi, S.B. Cinefra, Free vibration of variable-thickness plates via adaptive finite elements - ScienceDirect, 2024, https://www. sciencedirect.com/science/article/pii/S0022460X24000993.

[21] C.H. Thai, T.N. Nguyen, T. Rabczuk, H. Nguyen-Xuan, An improved moving kriging meshfree method for plate analysis using a refined plate theory, Comput. Struct. 176 (2016) 34–49, http://dx.doi.org/10.1016/J.COMPSTRUC.2016.07. 009.

[22] P. Xia, S.Y. Long, H.X. Cui, G.Y. Li, The static and free vibration analysis of a nonhomogeneous moderately thick plate using the meshless local radial point interpolation method, Eng. Anal. Bound. Elem. 33 (6) (2009) 770–777, http://dx.doi.org/10.1016/J.ENGANABOUND.2009.01.001.

[23] H.H. Phan-Dao, A meshfree radial point interpolation method for free vibration of laminated composite plates analysis based on layerwise theory, Procedia Eng. 142 (2016) 349–356.

[24] T.Y. Wu, G.R. Liu, Free vibration analysis of circular plates with variable thickness by the generalized differential quadrature rule. International, J. Solids Struct. 38 (44–45) (2001) 7967–7980, http://dx.doi.org/10.1016/S0020-7683(01)00077-4.

[25] Y.M. Grigorenko, L.S. Rozhok, Stress–Strain analysis of rectangular plates with a variable thickness and constant weight, Internat. Appl. Mech. 38 (2002) 167–173, http://dx.doi.org/10.1023/A:1015708810141.

[26] Zenkour A.M., Exact mixed-classical solutions for the bending analysis of shear deformable rectangular plates, Appl. Math. Model. 27 (7) (2003) 515–534, http://dx.doi.org/10.1016/S0307-904X(03)00046-5.

[27] Ashour A.S., Vibration of variable thickness plates with edges elastically restrained against translation and rotation, Thin-Walled Struct. 42 (1) (2004) 1–24, http://dx.doi.org/10.1016/S0263-8231(03)00127-7.

[28] I. Shufrin, M. Eisenberger, Vibration of shear deformable plates with variable thickness — first-order and higher-order analyses, J. Sound Vib. 290 (1–2) (2006) 465–489, http://dx.doi.org/10.1016/J.JSV.2005.04.003.

[29] P. Malekzadeh, S.A. Shahpari, Free vibration analysis of variable thickness thin and moderately thick plates with elastically restrained edges by DQM, Thin-Walled Struct. 43 (7) (2005) 1037–1050, http://dx.doi.org/10.1016/J.TWS.2004.11.008.

[30] S.A. Eftekhari, A.A. Jafari, High accuracy mixed finite element-ritz formulation for free vibration analysis of plates with general boundary conditions, Appl. Math. Comput. 219 (3) (2012) 1312–1344, http://dx.doi.org/10.1016/J.AMC.2012.07.039.

[31] N. Fantuzzi, M. Bacciocchi, F. Tornabene, E. Viola, AJM Ferreira, Radial basis functions based on differential quadrature method for the free vibration analysis of laminated composite arbitrarily shaped plates, Compos. Part B Eng. 78 (2015) 65–78.

[32] Yepeng Xu, Ding Zhou, Kefu Liu, Three-dimensional thermoelastic analysis of rectangular plates with variable thickness subjected to thermomechanical loads, J. Therm. Stresses 33 (12) (2010) 1136–1155.

[33] I. Shufrin, M. Eisenberger, Vibration of shear deformable plates with variable thickness - first-order and higher-order analyses, J. Sound Vib. 290 (1–2) (2006) 465–489.

[34] M.C. Moruzzi, M. Cinefra, S. Bagassi, Free vibration of variable-thickness plates via adaptive finite elements, J. Sound Vib. 577 (2024) 118336, http://dx.doi.org/10.1016/j.jsv.2024.118336.

[35] G.R. Liu, Meshfree Methods, Moving beyond the Finite Element Method, second ed. 2009, http://dx.doi.org/10.1201/9781420082104, Meshfree Methods.

[36] R. Pilafkan, P.D. Folkow, M. Darvizeh, A. Darvizeh, Three dimensional frequency analysis of bidirectional functionally graded thick cylindrical shells using a radial point interpolation method (RPIM), Eur. J. Mech. A Solids 39 (2013) 26–34, http://dx.doi.org/10.1016/J.EUROMECHSOL.2012.09.014.

[37] G. Jin, Z. Su, S. Shi, T. Ye, S. Gao, Three-dimensional exact solution for the free vibration of arbitrarily thick functionally graded rectangular plates with general boundary conditions, Compos. Struct. 108 (1) (2014) 565–577.

[38] K. Itakura, Free vibration analysis of thick skewed plates having arbitrary boundary conditions, J. Struct. Const. Eng. 492 (1997) 37–45.

[39] K.M. Liew, K.C. Hung, K.M. Lim, A continuum three-dimensional vibration analysis of thick rectangular plates, Int. J. Soilds Struct. 30 (1993) 3357–3379.

[40] S.M. Ibrahim, S.H. Alsayed, H. Abbas, E. Carrera, Y.A. Al-salloum, T.H. Almusallam, Free vibration of tapered beams and plates based on unified beam theory, 2012, p. 2014.